High-temperature kinetic and thermodynamic models for nitrogen plasmas

Élio Cordeiro Pereira
elio.pereira@ist.utl.pt

Instituto Superior Técnico, Lisboa, Portugal

February 2021

Abstract

The conditions of thermal, chemical and radiative non-equilibrium attained in a pure N_2 gas subjected to a strong shock wave were quantified using vibronic-specific state-to-state models. The Forced-Harmonic-Oscillator model (FHO) was employed in the computation of rate coefficients for vibrational transition and dissociation of N_2 and N_2^+ by heavy particle impact. Thermal dissociation rate coefficients of N_2(X) by collisions with N_2 and N were obtained and compared with state-of-the-art experimental results, showing an agreeability between -59.9 and $8.9\,\%$, and between -80.9 and $-36.1\,\%$ for the former and latter interactions, respectively. An extension of the Landau-Zener and Rosen-Zener-Demkov models to vibronic transitions of molecular particles by heavy particle impact was found to be impractical, and an exponential gap law was ultimately preferred. By fitting the curve that represents the law to experimentally obtained values for the respective rate coefficients, deviations by as much as one order magnitude were obtained, showing some crudeness of the model. Shots 19, 20 and 40 of the test 62 of the Ames Electric Arc Shock Tube (EAST) were simulated using the SPARK code. The experimental radiation variables were underestimated by one to two orders of magnitude, and sensibility tests performed on the rate coefficients weren't successful in getting a reasonable agreeability. The numerical simulations correctly predicted the shape of the radiative intensities profiles of the low speed shot but not the plateaus which proceeded peaks in the case of the medium and high speed shots. Strong evidence was found for such discrepancies resulting from the non-modelling of heat transfer by radiation within the test gas, and possibly, between the driver gas (as well as the driver arc) and the test gas.

Keywords: Atmospheric entry, Aerothermodynamics, Nitrogen plasma, State-to-state, Radiation, Shock tube

1. Introduction

1.1. The post-shock physical phenomena occurring in an atmospheric entry

When a blunt body from the outer space enters the atmosphere of a planet, it produces a strong detached shock wave causing an abrupt increase in temperature, pressure and density of the gas immediately downstream of the wave. The above-mentioned temperature is associated with the translational energy mode of the particles, being called heavy particle[1] translational temperature, $T_{\mathrm{tr_h}}$. The abrupt increase in heavy particle translational temperature leads to an almost simultaneous excitation of the rotational energy mode of the molecular particles. Hence, heavy particle translational-rotational equilibrium is usually assumed to occur immediately downstream of the shock wave and a heavy particle translational-rotational temperature may be defined [10]: $T_{\mathrm{tr_h\text{-}rot}} = T_{\mathrm{tr_h}} = T_{\mathrm{rot}}$. Vibrational excitation, electronic excitation and dissociation follows, the latter producing atomic particles in the flow. The atomic particles may then suffer associative ionisation, which in their turn, produce molecular ions and free electrons - the gas should now be called a plasma. The electrons quite effectively excite the electronic levels of the particles [10]. These excited particles may then de-excite through spontaneous emission, producing a radiation field in the medium. Other types of radiative transitions could occur, namely induced emission, photoionisation, photodissociation, bremsstrahlung and the respective reverse processes.

[1] Let's assume here that the atmosphere gas is solely composed by heavy particles.

1.2. The case of nitrogen plasmas

In this work, the post-shock conditions obtained from a pure nitrogen gas were studied. The

chemical reactions may be such that a significant fraction of the molecular nitrogen N_2 is transformed into at least four species: molecular nitrogen ion N_2^+, atomic nitrogen N, atomic nitrogen ion N^+ and free electron e^-. Molecular nitrogen is the main component of air, which below the Kármán line ($\sim 100\,\text{km}$), contributes with a mole fraction of 78.08 %. By restricting the study to the sole components of the mixture, one may divide the difficult task of modelling air into simpler ones. The whole mixture would then be described by the combination of the resultant models.

2. Literature Review

2.1. State-of-the-art of the thermodynamic models

The flow obtained in atmospheric entries is in thermal non-equilibrium, i.e. the various energy modes of the particles aren't in equilibrium with each other, and a single temperature T can't solely describe their energy. Instead, temperatures for each energy mode or sets of energy modes need to be regarded. It is here that multi-temperature models, such as the well-known Park's two-temperature and Lee's three-temperature models take their place. The former accounts the above-mention heavy particle translational-rotational temperature $T_{\text{tr}_\text{h}\text{-rot}}$, and a vibrational-electronic-free electron translational temperature $T_{\text{vib-el-tr}_\text{e}} = T_{\text{vib}} = T_{\text{el}} = T_{\text{tr}_\text{e}}$. The latter is more general than the former by stating a vibrational temperature T_{vib} and an electronic-free electron translational temperature $T_{\text{el-tr}_\text{e}} = T_{\text{el}} = T_{\text{tr}_\text{e}}$, beyond $T_{\text{tr}_\text{h}\text{-rot}}$. Park points out that numerical results obtained through multi-temperature models are significantly more agreeable with the experimental ones for the post-shock conditions than the single-temperature models, which assume thermal equilibrium. Several works such as the ones of Candler, Hornung and Lobb evidenced that the single-temperature model predicts the flow to be closer to thermodynamic equilibrium than it actually is. There are circumstances in which not even multi-temperature models may properly quantify the physical phenomena: the populations of the electronic, vibrational or even rotational energy levels may not follow Boltzmann distributions, and temperatures can't be assigned to them. This behaviour had been observed by Candler et al. and Munafó et al. For such cases, the so-called state-to-state models (or collisional-radiative models), which treat each energy level individually, need to be employed. In this work a vibronic-specific state-to-state model was regarded, which is electronic and vibrational-specific but not rotational-specific - as aren't the most part of the state-to-state models applied in the current days.

2.2. State-of-the-art of the kinetic models

One important kinetic process that will be further addressed in this work is the vibrational transition of molecular particles by heavy particle impact. Such phenomena may be quantified using the well-known Schwartz-Slawsky-Herzfeld model (SSH). This is a semi-classical model derived under a first-order perturbation theory (FOPT) approach, assuming collinearity of the collision, harmonicity of the molecular particles, and an exponential repulsive interaction potential. Due to the FOPT approach, only single vibrational energy level jumps are considered to occur, which is solely true for cases of small collisional speeds. The model shouldn't therefore be employed in numerical simulations of entry post-shock flows, due to the very high heavy particle translational temperatures attained in those conditions. The most precise models include the exact quantum mechanical models, like the one suggested by Secrest and Johnson, and Quasi-Classical Trajectory models (QCT), like the one developed by Billing. These models require, however, a considerable amount of computational resources, limiting their applicability. An alternative model which is much more accurate than the SSH model, and at the same time more practical than the two above-mentioned, is the Forced Harmonic Oscillator model (FHO) [1]. This is a non-perturbative semi-classical model being originally conceived by Kerner and Treanor for the case of molecular particle-atomic particle collision. It was then generalised for the case of molecular particle-molecular particle collision by Zelechow et al., and modified by Adamovich et al. [1] to account the anharmonicity of the molecular particles, the attractive long-range part of the interaction potential, the possible non-collinearity of the collision, the case in which the molecular particles are non-identical, and energy conservation. The developed model was shown to agree considerable well with the results obtained through the state-of-the-art Billing's model.

Another important kinetic process that will be further addressed in this work is the vibronic transition of molecular particles by heavy particle impact. There are two well-known theoretical models which deal with the homologous processes for the case of atomic particles - the electronic transitions of atomic particles by atomic particle impact: the Landau-Zener model [7, 13] and Rosen-Zener-Demkov model [5, 11]. It will be studied in this work the possibility of these models being extended to the case of vibronic transitions of molecular particles by heavy particles.

3. Background

3.1. The kinetic rate coefficient

Let's consider a process resulting from a collision between two heavy particles, A and B, producing ν'_{C} particles C and possibly others:

$$\mathrm{A} + \mathrm{B} \underset{k_b}{\overset{k_f}{\rightleftharpoons}} \nu'_{\mathrm{C}}\mathrm{C} + \cdots . \tag{1}$$

The forward rate coefficient of this process is defined as $k_f(T_{\mathrm{tr_h}})$ such that the rate of change of the amount concentration of C particles, [C], due to this same process in the forward direction, is given by

$$\left(\frac{d\,[\mathrm{C}]}{dt}\right)_f = (\nu'_{\mathrm{C}} - \nu_{\mathrm{C}})\, k_f(T_{\mathrm{tr_h}})[\mathrm{A}][\mathrm{B}] . \tag{2}$$

In (2), ν_{C} is the stoichiometric coefficient associated with the species C at the reactants side (note that it may not be null if C is identical to A or B). The rate coefficient depends on the respective process cross sections $\sigma_p(v)$ through

$$k_f = \int_0^\infty \sigma_p(v) f(v, T_{\mathrm{tr_h}})\, dv , \tag{3}$$

being v the relative speed of the collision partners, and $f(v, T_{\mathrm{tr_h}})$ the distribution of relative speeds. According to the Kinetic Theory of Gases [12], the latter is given by

$$f(v, T_{\mathrm{tr_h}}) = \frac{4\pi}{1+\delta_{\mathrm{AB}}} \left(\frac{\mu}{2\pi k_B T_{\mathrm{tr_h}}}\right)^{\frac{3}{2}} v^3 e^{-\frac{\mu v^2}{2k_B T_{\mathrm{tr_h}}}} , \tag{4}$$

where k_B is the Boltzmann constant, $\mu = m_{\mathrm{A}} \cdot m_{\mathrm{B}}/(m_{\mathrm{A}} + m_{\mathrm{B}})$ is the reduced mass of the collision partners, and δ_{AB} is a Kronecker delta giving 1 if A and B are identical, and 0 if not. An average process cross section $\sigma_{p,\mathrm{av}}(T_{\mathrm{tr_h}})$, corresponding to the average of $\sigma_p(v)$ with respect to $f(v, T_{\mathrm{tr_h}})$, may be defined, allowing one to rewrite (3) as

$$k_f(T_{\mathrm{tr_h}}) = \frac{\sigma_{p,\mathrm{av}}(T_{\mathrm{tr_h}})}{1+\delta_{\mathrm{AB}}} \sqrt{\frac{8k_B T_{\mathrm{tr_h}}}{\pi\mu}} . \tag{5}$$

The backward rate coefficient $k_b(T_{\mathrm{tr_h}})$ which is associated with the reverse direction of the process can be computed by analysing the case of thermodynamic equilibrium and obtaining the so-called equilibrium constant $K(T_{\mathrm{tr_h}})$ [12].

For the case in which one of the collision partners corresponds to a free electron e^-, it may be shown that the respective associated quantities are the ones given above with μ substituted by the electron mass m_{e}, and $T_{\mathrm{tr_h}}$ by the free electron translational temperature $T_{\mathrm{tr_e}}$ [10].

3.2. The Forced-Harmonic-Oscillator model

The FHO model adapted by Adamovich et al. [1] states that the probability of a molecular particle AB transiting from the n-th to the m-th vibrational level, by collision with an atomic particle C, corresponds to

$$P_n^m = n!m!\eta_0^{n+m} e^{-\eta_0} \left(\sum_{k=0}^{l} \frac{(-1)^k \eta_0^{-k}}{(n-k)!(m-k)!k!}\right)^2 , \tag{6}$$

where η_0 is given by

$$\eta_0 = \frac{8\pi^2\omega\tilde{m}^2\gamma^2}{\hbar\mu\alpha^2} \operatorname{csch}^2\left(\frac{2\pi\omega}{\alpha v_0}\right) \cosh^2\left[\frac{2\pi\omega}{\alpha v_0}\left(\frac{1}{2} + \frac{\phi}{\pi}\right)\right] . \tag{7}$$

In (7), $\phi = \arctan\left(\sqrt{E_{\mathrm{M}}/\frac{1}{2}\tilde{m}v_0^2}\right)$, E_{M} is the well depth of the Morse interaction potential, $\tilde{m}$ the reduced mass of the combination of the colliding particles, and v_0 the initial relative speed of collision. Also, $\hbar$ is the reduced Planck constant, ω is the natural angular frequency of the molecular particle, $\gamma = m_{\mathrm{A}}/(m_{\mathrm{A}} + m_{\mathrm{B}})$ is a mass parameter, μ is the reduced mass of the molecular particle, and α is the inverse length parameter of the Morse interaction potential.

According to Adamovich et al [1], if $T_{\mathrm{tr_h}} \gg T_{\mathrm{vib}}$ (which usually happens immediately downstream of a strong shock wave), the probability of vibrational transition of the colliding molecular particles AB e CD, from v_1-th to the v'_1-th vibrational level of the former, and from v_2-th to the v'_2-th vibrational level of the latter, can be approximated by a multiplication of two uncoupled probabilities:

$$P_{v_1,v_2}^{v'_1,v'_2} = P_{v_1}^{v'_1} \cdot P_{v_2}^{v'_2} , \tag{8}$$

being $P_{v_1}^{v'_1}$ and $P_{v_2}^{v'_2}$ given by (6).

Dissociation of a molecular particle by heavy-particle impact may be described by the FHO model allied with the mechanism proposed by Macheret and Adamovich [8]: dissociation is consider to occur when the final vibrational level v' exceeds the dissociation limit. The probability of dissociation is then defined as $P_v^D = \sum_{v' \geq v_D} P_v^{v'}$, being v_D the first vibrational level above the dissociation limit. The number of final vibrational levels v' which are regarded in the sum is a free parameter and may be conveniently chosen to calibrate the dissociation probability.

It's important to note that all of the above-mentioned formulae need to be corrected to account the anharmonicity of the molecular particles, the non-collinearity of the collisions, and energy conservation. Such corrections are detailed in the works of Adamovich et al. [1].

3.3. The Landau-Zener and Rosen-Zener-Demkov models

The Landau-Zener [7,13] and Rosen-Zener-Demkov [5, 11] models may be used to quantify electronic transitions of atomic particles by collision with other atomic particles. They correspond to semi-classical models valid under the so-called adiabatic approximation and the two-states approximation. When two atomic particles approach each other they form a quasi-molecular particle, whose respective interaction nuclear potential corresponds to the one of an equivalent molecular particle composed by the same two particles. If the interaction nuclear potential curve (having the internuclear distance as parameter) crosses another or performs an "avoided crossing", there's a probability of the system to transit to that other curve. After departing, the atomic particles will be found in the electronic levels associated with the dissociation products of a molecular particle having as interaction nuclear potential the last acquired one. The Landau-Zener model may be used to compute the probability of electronic transition in such cases. Conversely, the Rosen-Zener-Demkov model may be used if the two interaction nuclear potential curves solely get near each other at the large internuclear distances.

The possibility of extension of both Landau-Zener and Rosen-Zener-Demkov models to vibronic transitions of molecular particles by heavy particle impact beyond electronic transitions of atomic particles by atomic particle impact, have been put into question recently, namely through the works of Kirillov et al. Kirillov derived some simplistic formulae for the two mechanisms. However, not only the derivation of the analytic expressions is somewhat puzzling, but the approach per se lacks physical coherency. For instance, the relative speed of the atomic particles considered in the Landau-Zener and Rosen-Zener-Demkov models is interpreted by Kirillov as the relative speed of the collision partners in the molecular particle-heavy particle collision, while, simultaneously, the internuclear potential curves are interpreted as the ones for nuclei of the same molecular particle instead the ones for nuclei of both collision partners. A more rightful way of determining the probability of vibronic transition is by solving the classical equations of motion of all nuclei and applying the Landau-Zener model at the internuclear distances associated with the crossing or pseudo-crossing of the potential curves of the molecular particles - the so-called Trajectory Surface Hopping Approach (TSHA). However, the values of the parameters required by this method for the case of the vibronic transitions of N_2 and N_2^+ aren't currently known, and, therefore, the approach can't be regarded in this work.

After a prudent review of the literature, it was decided to use an "exponential gap" law model for the average process cross section $\sigma_{p,\mathrm{av}}$ having the vibronic and thermal dependences suggested by Bachmann et al. [2] and Katayama et al. [6], respectively, i.e.

$$\sigma_{p,\mathrm{av}}\left(T_{\mathrm{tr_h}}\right) = \sigma_0' \, e^{-\frac{|\Delta E|}{E_0} + \frac{\varepsilon}{k_B T_{\mathrm{tr_h}}}} \ , \tag{9}$$

being $\sigma_0' = \sigma_0 e^{-\frac{\varepsilon}{k_B T_{\mathrm{ref}}}}$, where σ_0 is a characteristic cross section, ε is the well depth of the interaction potential, and T_{ref} is a reference temperature. Also, ΔE is the energy defect (the difference between the initial and final internal energies of the collision partners), and E_0 is a characteristic energy.

3.4. Fluid flow governing equations under the 0D and 1D vibronic-specific state-to-state models

In this work, numerical simulations of post-shock flows obtained in the test 62 of EAST [3] were performed with objective of validating the conceived database of kinetic processes. A zero-dimensional approximation was initially regarded since it is a simpler approach requiring less computational efforts. In this model, the effects of spatial variation of the physical quantities on the properties of an element of fluid are assumed to be negligible. Figuratively, this approximation is equivalent to constrain the element of fluid to a transparent fixed-volume box, and to remove it from the flow. The element of fluid would not be subjected to momentum transfer, to transport phenomena - mass diffusion, heat conduction and viscosity - neither would receive radiative energy from the complementary system. An Euler one-dimensional approximation was also considered. In this model, the flow is assumed to be permanent and, similarly to the zero-dimensional approximation, the transport phenomena and radiation transfer between elements of fluid are neglected. One more equation needs to be solved, which is with respect to momentum transfer. Note that in both models, emission of radiative energy (solely by spontaneous emission) and auto-absorption (i.e. absorption by the same emitting source) was considered and represented by a volumetric radiative energy source $\dot{\Omega}_{\mathrm{rad}}$ in the balance equation of total energy. This term is given by

$$\dot{\Omega}_{\mathrm{rad}} = hc \left(\sum_{\mathrm{se}} \Lambda_{s,e,v}^{e',v'} A_{s,e,v}^{e',v'} \, n_{s,e,v} \int_0^\infty \frac{\phi_{\lambda,s,e,v}^{e',v'}}{\lambda} \, d\lambda \right) . \tag{10}$$

In (10), h corresponds to the Planck constant, c is the speed of light, $A_{s,e,v}^{e',v'}$ is the Einstein coefficient for spontaneous emission from the vibronic level

(e, v) to (e', v'), $\phi^{e',v'}_{\lambda,s,e,v}$ is the respective line-shape factor, $n_{s,e,v}$ is the number density, and λ is the wavelength. The quantity $\Lambda^{e',v'}_{s,e,v}$ is the so-called escape factor, corresponding to the fraction of the emitted photons due to spontaneous emissions from (e, v) to (e', v') which escape from the system (i.e. not auto-absorbed). The sum in (10) is done in all the spontaneous emission processes. In this work, the line-shape factor $\phi^{e',v'}_{\lambda,s,e,v}$ was considered to be the result of four contributions: Doppler, collisional, Stark, and resonance broadening.

The unknowns of the equations for the zero-dimensional model are the mass fractions $c_{s,v,e}$ ($\forall s$, v, and e), and temperatures $T_{\mathrm{tr_h}}$ and $T_{\mathrm{tr_e}}$. And the unknowns of the equations for the one-dimensional model are all of these plus the x-component of the flow velocity vector u. Note that in the case of the zero-dimensional model, the mixture mass density ρ is an invariable and its value may be taken as the one attributed with respect to the initial conditions. In the case of the one-dimensional model, ρ is given by a global balance equation for mass which also depends on u. Initial values need to be assigned to $c_{s,v,e}$, $T_{\mathrm{tr_h}}$, $T_{\mathrm{tr_e}}$, u and ρ. These are associated with the conditions of the post-shock flow immediately downstream of the shock wave - labelled here by the number "2" - and may be determined through the knowledge of the upstream conditions - labelled here by the symbol "∞". Since the flow from ∞ to 2 is "frozen", one has $c_{s,v,e,2} = c_{s,v,e,\infty}$. And the quantities ρ_2, $T_{\mathrm{tr_h},2}$ and u_2 are given by the well-known Rankine-Hugoniot jump conditions:

$$\rho_2 = \frac{(\gamma+1)\,M_\infty^2}{(\gamma-1)\,M_\infty^2+2}\rho_\infty \ , \tag{11}$$

$$T_{\mathrm{tr_h},2} = \frac{\left[(\gamma-1)\,M_\infty^2+2\right]\left[2\gamma M_\infty^2-(\gamma-1)\right]}{(\gamma+1)^2\,M_\infty^2}T_\infty \ , \tag{12}$$

$$u_2 = \frac{(\gamma-1)\,M_\infty^2+2}{(\gamma+1)\,M_\infty^2}u_\infty \ , \tag{13}$$

being M_∞ the upstream Mach number, and γ the ratio of specific heats. For the case of the zero-dimensional model, the flow speed downstream of the shock wave u was assumed to be constant and equal to the immediately downstream value u_2, allowing one to express the position of the element of fluid as $x = u_2 \cdot t$. The hypothesis $T_{\mathrm{tr_h},2} = T_{\mathrm{tr_e},2}$ was taken, as also done by Kadochnikov and Arsentiev.

4. Set-up of the database of kinetic processes

4.1. The species energy levels

The electronic energies of the molecular nitrogen N_2 and molecular nitrogen ion N_2^+ were taken from the literature. A total of 15 electronic levels were considered for the case of N_2 - X, A, B, W, B′, a′, a, w, A′, C, b, c_3, c_4', b′ and o_3 - and 5 for the case of N_2^+ - X, A, B, D and C. The respective vibrational energies of each of the considered electronic levels, were obtained using the Fourier Grid Hamiltonian method. The required potential curves were generated by implementation of the Rydberg-Klein-Rees method allied with extrapolation. The electronic energies of the atomic nitrogen N and atomic nitrogen ion N^+ were taken from the National Institute of Standards and Technology (NIST) database, and a lumping procedure was performed on them with the objective of disregarding their fine structure.

4.2. Thermal dissociation of N_2(X) by collisions with N_2 and N

Rate coefficients for dissociation of $N_2(X, v)$ by collisions with N_2 and N were obtained using the FHO model. Let these be denoted by $k^D_{\mathrm{N_2},v}(T_{\mathrm{tr_h}})$ and $k^D_{\mathrm{N},v}(T_{\mathrm{tr_h}})$, respectively. Thermal[2] dissociation rate coefficients of N_2(X) by collision with N_2 and N - $k^D_{\mathrm{N_2}}(T)$ and $k^D_{\mathrm{N}}(T)$ - may be shown to be given by

$$k^D_{\mathrm{M}}(T) = \sum_v \frac{e^{-\frac{\epsilon_{\mathrm{vib},v}}{k_B T}}}{Q_{\mathrm{vib}}(T)} k^D_{\mathrm{M},v}(T) \ , \tag{14}$$

where $\mathrm{M} \in \{\mathrm{N}, \mathrm{N_2}\}$ is the collision partner, $\epsilon_{\mathrm{vib},v}$ is the sensible vibrational energy of the v-th vibrational level, and $Q_{\mathrm{vib}}(T)$ is the vibrational partition function. The number of regarded vibrational levels above the dissociation limit were chosen in order to minimise the deviation between the computed rates and the state-of-the-art ones computed by Park [9] (which are based on experimental works). Figures 1 and 2 show the FHO thermal dissociation rates obtained in this work, the ones of Park, as well as QCT rates recently computed by other authors. It was found that the FHO model underestimates the Park results at the low temperatures and overestimate them at the high ones. In the experimentally valid region (thick part of the lines), the numerical rates deviate between -59.9% and 8.9% from the Park ones for the case $\mathrm{M} = \mathrm{N_2}$, and between -80.9% and -36.1% for the case $\mathrm{M} = \mathrm{N}$. Furthermore, the FHO model underestimate all the QCT results for the case $\mathrm{M} = \mathrm{N_2}$, with extreme deviations of -44.3% and -56.5% from the values of Bender et al. and Macdonald et al., respectively. For the case $\mathrm{M} = \mathrm{N}$, the FHO results underestimate the QCT results at the lower temperatures and overestimate them at the higher ones, with extreme deviations of 46.2% and 37.9% from the values of Esposito and Capitelli and Jaffe et al., respectively.

[2] A thermal rate coefficient corresponds to a rate coefficient evaluated at thermal equilibrium, hence depending solely on the equilibrium temperature T.

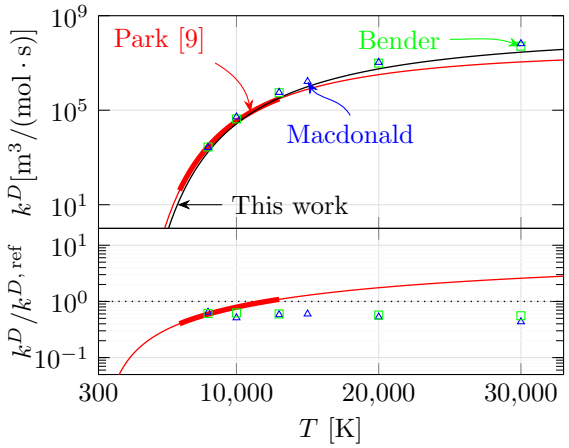

Figure 1: Thermal dissociation rates of N_2(X) by collision with N_2, and ratio between the FHO values and the others.

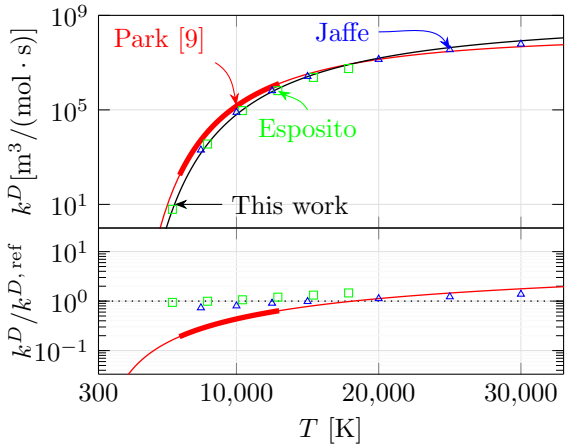

Figure 2: Thermal dissociation rates of N_2(X) by collision with N, and ratio between the FHO values and the others.

4.3. Vibronic transitions of N_2 by heavy particle impact

The model for the average process cross section (9) was used in this work to compute the respective rate coefficients of different vibronic transitions through curve fitting of data obtained in room temperature experiments. The regarded vibronic transitions were the ones of N_2(A) to N_2(B) and of N_2(W) to N_2(B) by collision with N_2(X) and N(0)[3], of N_2(A) to N_2(B) and N_2(C) by collision with N_2(A) which in its turn transits to N_2(X), and of N_2(A) to N_2(X) by collision with N_2(X) and N(0) which in its turn transits to N(2). It was found that in some cases the model was too crude to predict the particular behaviour of the experimental data. The obtained fitted curves departed from the points values as much as by one order of magnitude.

[3]In this work, the electronic levels of atomic particles will be labelled by integer numbers 0, 1, ...

5. Results of numerical simulations of post-shock flows generated by a shock tube

From the 17 shots benchmarked by Brandis and Cruden [3], 3 were chosen to be numerically simulated: shots 40 (with $u_\infty = 6.88$ m/s), 19 (with $u_\infty = 10.32$ m/s), and 20 (with $u_\infty = 11.16$ m/s). These differ on the upstream flow speed u_∞, and are of benchmark quality in the four regarded wavelength intervals (VUV, "Blue", "Red", and IR). Brandis and Cruden issue experimentally obtained values for the instrumentally resolved radiative intensities $\hat{I}^l$ and non-equilibrium metrics $\hat{I}^{\mathrm{ne},l}_\lambda$, with $l \in \{\mathrm{VUV}, \text{"Blue"}, \text{"Red"}, \mathrm{IR}\}$. These two variables are related to the instrumentally resolved specific radiative intensity $\hat{I}_\lambda(x,\lambda)$ through

$$\hat{I}^l(x) = \int_{\lambda^l_{\min}}^{\lambda^l_{\max}} \hat{I}_\lambda(x,\lambda)\, d\lambda \ , \tag{15}$$

$$\hat{I}^{\mathrm{ne},l}_\lambda(\lambda) = \frac{1}{D}\int_{x^l_{\min}}^{x^l_{\max}} \hat{I}_\lambda(x,\lambda)\, dx \ , \tag{16}$$

respectively, being D the shock tube inner diameter. The values of the limits of integration $\lambda^l_{\min}$, $\lambda^l_{\max}$, $x^l_{\min}$ and $x^l_{\max}$ are supplied by Brandis and Cruden [3]. $\hat{I}_\lambda(x,\lambda)$ is in its turn related to the specific radiative intensity I_λ through a double convolution on an instrument line-shape factor $\hat{\phi}^{\mathrm{spe}}$ and a spatial resolution function $\hat{\phi}^{\mathrm{spa}}$ (also supplied by Brandis and Cruden).In this work, $I_\lambda(x,\lambda)$ was derived assuming an optically thin medium. An escape factor $\Lambda^{e',v'}_{s,e,v}$ was then added as a possible correction, resulting in

$$I_\lambda(x,\lambda) = \frac{hcD}{\lambda}\left[\sum_{\mathrm{se}} \Lambda^{e',v'}_{s,e,v}\frac{A^{e',v'}_{s,e,v}}{4\pi}\,\phi^{e',v'}_{s,e,v}(\lambda)\, n_{s,e,v}(x)\right] . \tag{17}$$

The peak values of the radiative intensities obtained from the Euler one-dimensional simulations were found to be between the double and the quintuple of the ones obtained from a zero-dimensional simulations, revealing the hypothesis of the momentum transfer being negligible (which is taken by the latter) to be invalid. The zero-dimensional simulations were then disregarded. Figures 3, 5, 7 and 9 show the contributions of the different spontaneous emission systems to the intrumentally resolved radiative intensities (solid coloured lines) as well as the sum of all of them (solid black lines), in the VUV, "Blue", "Red" and IR wavelength intervals, respectively, which were obtained from the one-dimensional simulations. The figures also show the intrumentally resolved radiative intensities obtained in the experiments (dotted black lines). The instrumentally resolved non-equilibrium metrics are in their turn presented by Figures 4, 6, 8 and 10, with the same symbolism.

The three graphs in each figure are with respect to the low speed (top one), medium (middle one), and high speed (bottom one) shots. It was found that the numerical features underestimated the experimental ones by one to two orders of magnitude. In order to make the numerical and and experimental results visually comparable in the figures, it was decided to consider two y-axes for each graph, being differently scaled, the left y-axis quantifying the numerical values, and the right y-axis quantifying the experimental values. The scales in the figures for the radiative intensities were chosen in order to make the heights of the peaks match each other. And the same was done for the case of the scales in the figures for the non-equilibrium metrics, with respect to peaks obtained by some particular spontaneous emissions processes (at $\lambda = 149$, 391, 869 and 940 nm in the VUV, "Blue", "Red" and IR wavelength intervals, respectively). One may now compare the obtained results in a relative way, that is, as if they had the same amplitudes.

In the case of the low speed shots, the numerical and experimental profiles of the radiative intensities correspond to sole peaks. The rising parts of peaks agree relatively well with the experimental ones, but not the falling parts which are steeper for the cases of the "Blue", "Red", and IR wavelength regions. Regarding the medium and high speed shots, the experimental profiles of the radiative intensities show plateaus proceeding peaks which aren't at all predicted by the numerical model. In the cases where the plateaus don't surpass the heights of the peaks, the shapes of the latter are remarkably well predicted. The numerically obtained non-equilibrium metrics depart significantly from the experimental ones. The contributions of atomic nitrogen N are found to be underestimated when compared to the contributions of the other spontaneous emission systems. Sets of groups of peaks can be discerned from the spectra, as from the experimental one, but the individual peaks don't

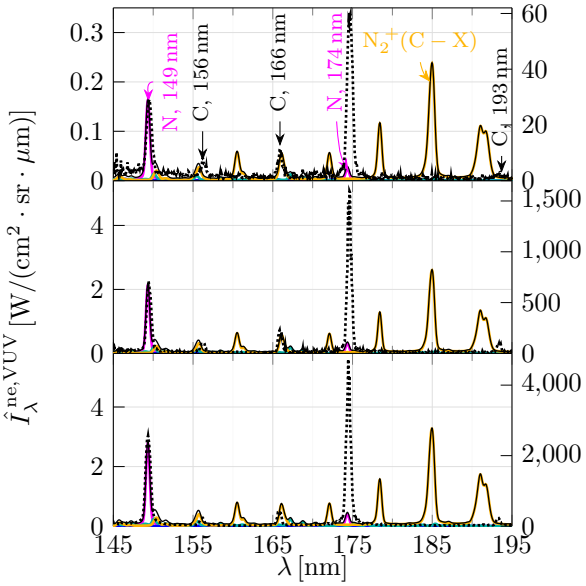

Figure 4: Numerical (solid lines) and experimental (dotted lines) instrumentally resolved non-equilibrium metrics $\hat{I}_\lambda^{ne,VUV}(x)$ obtained for the low, medium and high speed shots.

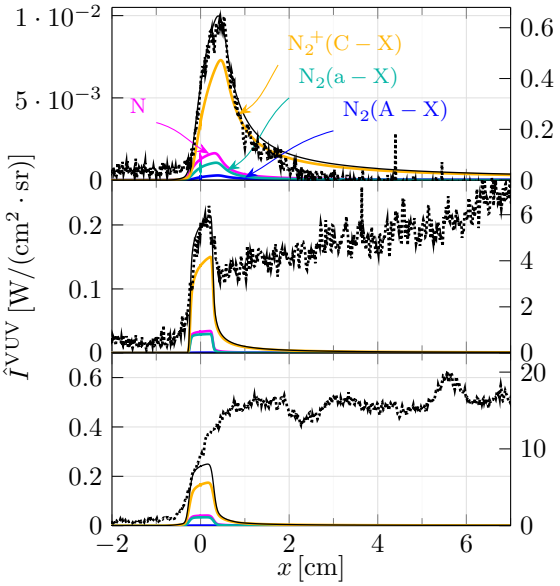

Figure 3: Numerical (solid lines) and experimental (dotted lines) instrumentally resolved radiative intensities $\hat{I}^{VUV}(x)$ obtained for the low, medium and high speed shots.

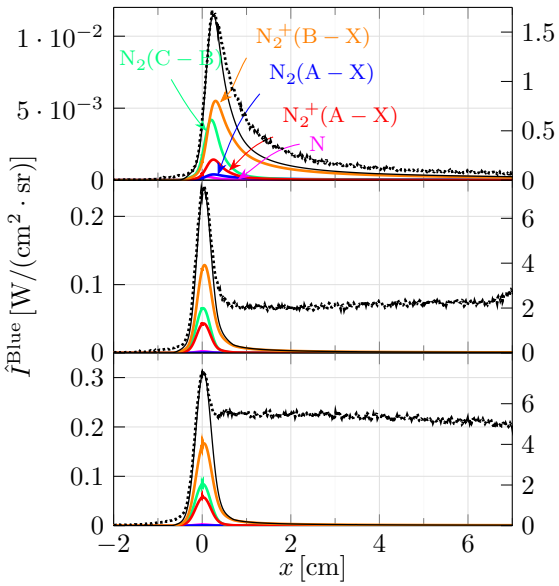

Figure 5: Numerical (solid lines) and experimental (dotted lines) instrumentally resolved radiative intensities $\hat{I}^{Blue}(x)$ obtained for the low, medium and high speed shots.

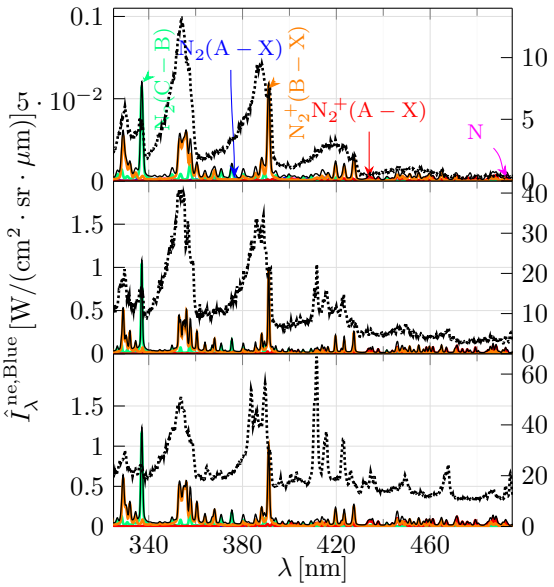

Figure 6: Numerical (solid lines) and experimental (dotted lines) instrumentally resolved non-equilibrium metrics $\hat{I}_\lambda^{\mathrm{ne,Blue}}(x)$ obtained for the low, medium and high speed shots.

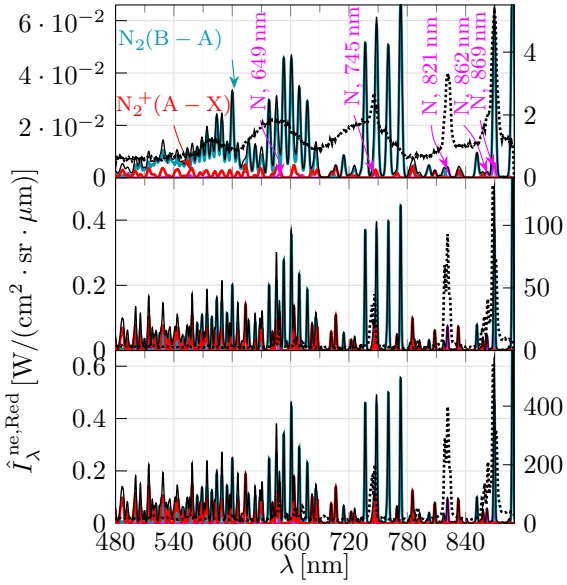

Figure 8: Numerical (solid lines) and experimental (dotted lines) instrumentally resolved non-equilibrium metrics $\hat{I}_\lambda^{\mathrm{ne,Red}}(x)$ obtained for the low, medium and high speed shots.

agree reasonably well with the experimental counterparts. The numerical spectra seems to be less smoother. This may in some part be due to the fact of the regarded Einstein coefficients being vibronic-specific and not rovibronic-specific, which reduces the number of peaks associated with the molecular spontaneous emission systems. The lumping procedure performed on the electronic levels of N also reduces the number of obtained peaks, and on the other hand, may turn the calibration of rate coefficients to be irrelevant in some cases. For instance, in the VUV wavelength interval, one finds the N peak at $\lambda = 149\,\mathrm{nm}$ to be higher than the one at $\lambda = 174\,\mathrm{nm}$ for the case of the numerical spectra, but lower for the case of the experimental one. A way of decreasing the height of the first peak and increasing the height of the second, is by decreasing the rate of excitation of N to the upper level of the system associated with the

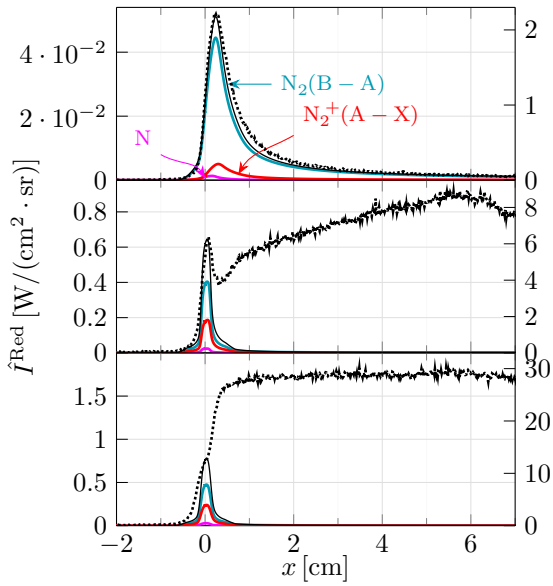

Figure 7: Numerical (solid lines) and experimental (dotted lines) instrumentally resolved radiative intensities $\hat{I}^{\mathrm{Red}}(x)$ obtained for the low, medium and high speed shots.

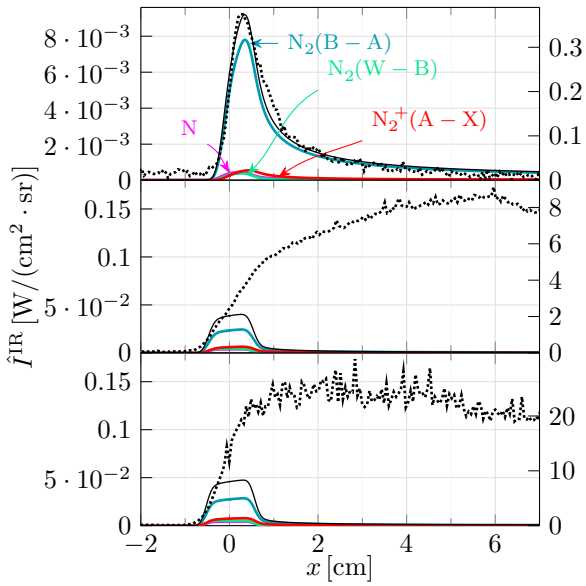

Figure 9: Numerical (solid lines) and experimental (dotted lines) instrumentally resolved radiative intensities $\hat{I}^{\mathrm{IR}}(x)$ obtained for the low, medium and high speed shots.

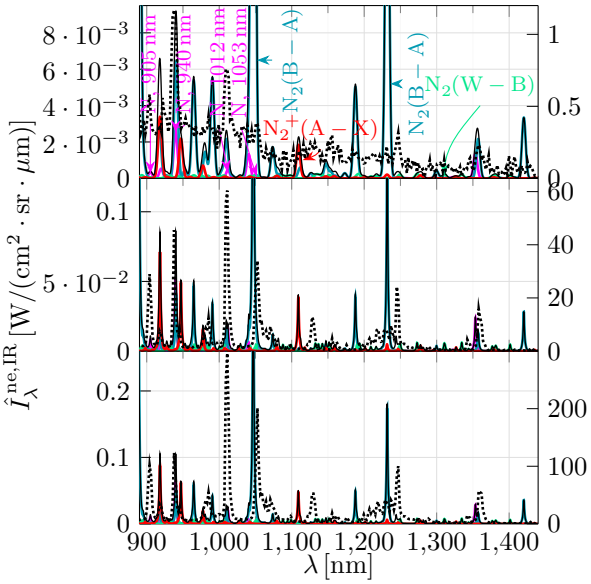

Figure 10: Numerical (solid lines) and experimental (dotted lines) instrumentally resolved non-equilibrium metrics $\hat{I}_\lambda^{ne,IR}(x)$ obtained for the low, medium and high speed shots.

former and increasing the one associated with the latter. However, the upper levels of the system associated with the two peaks are the same due to the lumping procedure, and changing the values of the rate coefficients for excitation would not make any difference in the ratio between the heights of the peaks. If the lumping procedure wasn't regarded, the first peak would correspond to a sum of three peaks and the second to a sum of four peaks, whose number of upper levels associated with the respective spontaneous emission systems would be two instead of one, allowing a possible calibration.

In the VUV spectra presented by Figure 4, three peaks which weren't predicted by the database appear. According to Cruden and Brandis [4] these are due to spontaneous emission of atomic carbon C - a contaminant species. The authors also reported evidence for the presence of another contaminant species: cyanogen radical CN and atomic hydrogen H. These ones express themselves in the other wavelength intervals. Note, however, that the contributions of the contaminants to the radiation variables appear to be much lesser than the ones of the species deriving from N_2.

Sensibility tests on different parameters of the simulations were performed, namely the consideration of escape factors $\Lambda^{VUV} = 0.1$, and 0.01 for the VUV radiation, changes of scale of the dissociation rates of N_2(X) by factors of 0.1 and 10, as well as changes of scale of the excitation rates of N by factors of 10 and 100. The consideration of escape factors led to a prevailing increase of the contributions of N to the radiation variables, and steeper profiles of radiative intensity which agree better with the experimental one for the case of the VUV radiation of the low speed shot. These improvements showed that the medium should be regarded as optically tick in the VUV wavelength interval, and not as optically thin. By decreasing the dissociation rates of N_2(X) the energy which was once spent in dissociation, was then used for excitation, mainly of N_2. The radiation variables increased, but the contributions of N to them were overshadowed by the ones of N_2, disagreeing with the experimental results. Conversely, by increasing the dissociation rates, the radiation variables decreased but the contributions of N were privileged over the ones of N_2, as in the experiment. Therefore, one cannot say that better results may be unequivocally attained by solely changing the dissociation rates of N_2(X). The increase of the excitation rates of N made the radiation variables to also increase. In fact, the contributions of N were so much enhanced that in the "Blue" region these prevailed over the contributions of N_2 and N_2^+, when in the experiment, the reverse happened. The profiles of radiative intensity got steeper, which also went in contradiction with the experimental results. One also cannot state that the sole increase of the excitation rates of N may unequivocally lead to better results.

Even by significantly changing the rate coefficients in the sensibility tests, the peaks of radiative intensity still departed by one to two orders of magnitude from the experimental ones.

Cruden and Brandis [4] inferred values for the final temperatures and mole fractions of the medium speed shot through an analysis of the radiation spectra. These were obtained by fitting the conditions of a hypothetical system such that the computed "Blue" and "Red" spectra matched the experimental ones, using the NEQAIR tool, at a x position for which the plateaus of radiative intensities occurred. With that objective, a two-temperature model - of temperatures $T_{\mathrm{tr_h-rot}}$ and $T_{\mathrm{vib-el-tr_e}}$ - was assumed, and the populations of some particular energy levels were additionally adjusted. The results of Cruden and Brandis show a stronger dissociation and ionisation with a lower cost of translational temperatures (these are several thousands of kelvins higher than the ones of this work) and a greater emission of radiation. Therefore, there's a strong evidence for the elements of fluid simulated in this work not receiving the amount of energy which they should. In fact, the transfer of heat by radiation between the different elements of fluid (hetero-absorption) was not modelled and may be one of the reasons for such discrepancies. It is only by performing simulations disregarding spontaneous

emission (therefore retaining the energy which was once lost through radiation) that the final mole fractions (except the one of N_2^+) and temperatures agree with the ones of Cruden and Brandis, endorsing even more the enunciated hypothesis.

Several studies in the literature stated that the so-called precursor phenomena, as well as the transfer of radiative energy from the driver gas and electric arc to the driven gas in shock tubes may be two possible causes of the significant underestimation of the radiation variables by numerical models as reported by other works.

6. Conclusions

In this work, a extensive set of vibronic energy levels for N_2, N_2^+, N and N^+, and a database of kinetic processes that relate them were built using the most up-to-date (in the limits of perception of the author) data available in the literature. Thermal dissociation rate coefficients of N_2(X) by collisions with N_2 and N were obtained using the FHO model, having the same order of magnitude as state-of-the-art experimental ones. Rate coefficients for several vibronic transition of N_2 were computed through an "exponential gap" law deviating as much as by one order of magnitude from experimental values, showing some crudeness of the model. The results of the shock tube simulations showed a significant underestimation of the radiation variables (by one to two orders of magnitude), and unprediction of the plateaus of radiative intensity occurring for the case of the higher speed shots. It's suspected that these deviations were due to the non-modelling of heat transfer by radiation within the driven gas - which requires the equation of radiative transfer to be solved - and possibly, between the driver gas (as well as the electric arc) and the driven gas. These should be accounted in the future.

Acknowledgements

The author would like to thank Prof. Mário Lino da Silva, Prof. Jorge Loureiro and Prof. Vasco Guerra from the IPFN group for the theoretical support, as well as Dr. Bruno Lopez from the University of Illinois Urbana-Champaign and the APPLAuSE PhD students Duarte Gonçalves, João Vargas and Ricardo Ferreira for their help regarding the implementation of the SPARK code.

References

[1] I. V. Adamovich, S. O. Macheret, J. W. Rich, and C. E. Treanor. Vibrational energy transfer rates using a forced harmonic oscillator model. *Journal of Thermophysics and Heat Transfer*, 12(1):57–65, Jan. 1998. doi:10.2514/2.6302.

[2] R. Bachmann, X. Li, C. Ottinger, A. F. Vilesov, and V. Wulfmeyer. Vibrational-state-to-state collision-induced intramolecular energy transfer $N_2(A^3\Sigma_u^+, v'' \rightarrow B^3\Pi_g, v')$. *The Journal of Chemical Physics*, 98(11):8606–8625, 1993. doi:10.1063/1.464469.

[3] A. M. Brandis and B. A. Cruden. Shock Tube Radiation Measurements in Nitrogen. In *2018 Joint Thermophysics and Heat Transfer Conference*, 2018. doi:10.2514/6.2018-3437.

[4] B. A. Cruden and A. M. Brandis. *Analysis of Shockwave Radiation Data in Nitrogen.* Jun 2019. doi:10.2514/6.2019-3359.

[5] Y. N. Demkov. Charge transfer at small resonance defects. *Sov. Phys. JETP*, 18(1):138–142, 1964.

[6] D. H. Katayama, A. V. Dentamaro, and J. A. Welsh. State specific electronic quenching rates for $^{14}N_2^+$ and $^{15}N_2^+$. *The Journal of Chemical Physics*, 87(12):6983–6987, 1987. doi:10.1063/1.453394.

[7] L. D. Landau. *Phys. Zts. Sov.*, 2(46), 1932.

[8] S. O. Macheret and I. V. Adamovich. Semiclassical modeling of state-specific dissociation rates in diatomic gases. *The Journal of Chemical Physics*, 113(17):7351–7361, 2000. doi:10.1063/1.1313386.

[9] C. Park. Two-temperature interpretation of dissociation rate data for N_2 and O_2. In *26th Aerospace Sciences Meeting*, January 1988. doi:10.2514/6.1988-458.

[10] C. Park. *Nonequilibrium Hypersonic Aerothermodynamics.* John Wiley and Sons Ltd, New York, United States, April 1990.

[11] N. Rosen and C. Zener. Double Stern-Gerlach Experiment and Related Collision Phenomena. *Phys. Rev.*, 40:502–507, May 1932. doi:10.1103/PhysRev.40.502.

[12] W. G. Vincenti and C. H. Kruger. *Introduction to physical gas dynamics.* John Wiley & Sons, 1965.

[13] C. Zener and R. H. Fowler. Non-adiabatic crossing of energy levels. *Proceedings of the Royal Society of London. Series A, Containing Papers of a Mathematical and Physical Character*, 137(833):696–702, 1932. doi:10.1098/rspa.1932.0165.